Progressive mainshock-aftershock damage in Christchurch, New Zealand

H.B. Mason

Oregon State University, Corvallis, Oregon, USA.

Z. Chen

University of Missouri at Kansas City, Kansas City, Missouri, USA.

2012 NZSEE Conference

ABSTRACT: Aftershocks following an earthquake can be damaging to the built environment, as observed in New Zealand during 2010 and 2011. In this paper, the aftershock sequence is discussed and a soil-foundation-structure numerical model is introduced. The numerical model represents a 9-story, inelastic, steel, eccentrically-braced frame structure founded on a shallowly-embedded mat foundation. Soil-foundation-structure interaction effects were explicitly considered by employing nonlinear Winkler springs. The model was subjected to the 22 February 2011 Christchurch Earthquake and two larger aftershocks, and the progressive seismic damage was tracked. Results show that for this type of structure, the seismic damage caused by the aftershocks is negligible compared to the mainshock. More modelling effort is needed to examine the progressive damage of other soil-foundation-structure models.

1 INTRODUCTION

Following an earthquake mainshock, smaller magnitude aftershocks are common. In general, the cumulative energy released from the aftershocks is only about 10% of the energy release of the mainshock (Lay & Wallace 1995). For this reason, aftershocks have often been ignored in seismic design and retrofitting. Aftershock sequences following the 4 September 2010 Darfield Earthquake in the Christchurch, New Zealand region, however, have shown that aftershock-induced damage should not be ignored. The observed aftershock damage has important implications for retrofitting New Zealand's current building stock, and updating current seismic design procedures. In addition, the lessons learned from New Zealand are applicable to other seismically-active areas characterized by shallow, crustal faulting (e.g., coastal California).

In this paper, the mainshock-aftershock sequence following the 4 September 2010 Darfield Earthquake is introduced. Within this sequence is the smaller mainshock-aftershock 'subsequence' that occurred after the 22 February 2011 Christchurch Earthquake, which caused much damage to the Christchurch city-centre, because of its short hypocentral distance. Next, we introduce a numerical model of a 9-story eccentrically-braced frame structure. In the modelling effort, we also consider the flexibility of the soil-foundation interface, and thus soil-foundation-structure interaction effects. This SFSI numerical model is used to predict progressive seismic damage from a mainshock-aftershock sequence. The key motivation behind this work is to understand the extent of aftershock damage after a significant mainshock. The time between the mainshock and the significant aftershocks is usually small (i.e., on the order of minutes and hours), so engineers usually cannot assess the extent of structural damage between the mainshock and aftershocks. Understanding the importance of aftershock-induced damage will be important to seismic engineers moving forward, as we strive to update the building codes. All dates and times given in this paper are in local New Zealand time. All earthquake data presented in this paper are from Geonet, and all reported magnitudes are local magnitudes.

2 METHODOLOGY

2.1 Earthquake motion sequence

When examining aftershock data, a contentious issue is the assumed geographic area (Bhattacharya et al. 2011); however, Kagan (2002) recommends that the linear extent of the examined area, L, be scaled with the mainshock magnitude, M_{ms}, as L (km) = $0.02 \cdot 10^{0.5Mms}$. For this study, the following latitude, longitude corners are chosen: (-44.20, 171.39); (-42.86, 171.39); (-42.86, 173.02); (-44.20, 173.02). This area spans about 75 km north, 30 km east, 75 km south, and 100 km west from the city-centre of Christchurch, and thus encompasses a total area of 130 km by 150 km (19,500 km^2).

Figure 1 shows the recorded earthquakes with epicentres in the chosen geographic area as a function of magnitude and time after the 4 September 2010 Darfield Earthquake (ending 31 January 2012). In developing this figure, a minimum magnitude of 3.5 is chosen. Figure 2 shows the cumulative number of earthquakes as a function of time. In developing this figure, a minimum magnitude of 2.5 is chosen. Figure 2 can be used to develop aftershock statistics (i.e., the Omori scaling law), which is outside the scope of this paper.

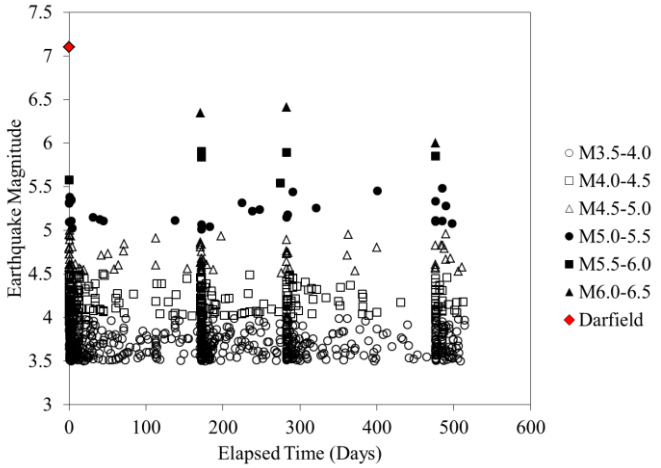

Figure 1. Distribution of earthquake magnitudes larger than 3.5 as a function of magnitude and elapsed time after the 4 September 2010 Darfield Earthquake within the latitude longitude range of: (-44.20, 171.39); (-42.86, 171.39); (-42.86, 173.02); (-44.20, 173.02)

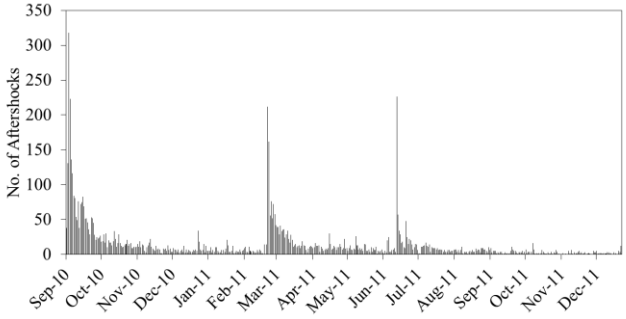

Figure 2. The number of aftershocks as a function of time after the 4 September 2010 Darfield Earthquake within the latitude longitude range of: (-44.20, 171.39); (-42.86, 171.39); (-42.86, 173.02); (-44.20, 173.02)

Figures 1 and 2 technically only show one mainshock-aftershock sequence, as the larger magnitude events (i.e., M6.3 2011/02/22; M6.4 2011/06/13; M6.0 2011/12/23) were aftershocks of the Darfield Earthquake (Bannister et al. 2011). However, our discussion focuses on the 22 February 2011 Christchurch Earthquake, and for engineering purposes, we consider this a separate mainshock-aftershock series, even though this is not strictly correct. More specifically, for performing the progressive damage simulations, the 22 February 2011 Christchurch mainshock and its largest two aftershocks are considered. The Christchurch Cathedral College (CCCC) seismic station, which is part

of the Canterbury regional strong motion network, is chosen for obtaining the recordings. The CCCC station is located in the Christchurch city-centre (-43.538085, 172.647427).

Table 1 provides details about the Christchurch mainshock, its M5.8 aftershock that followed 13 minutes afterward, and its M5.9 aftershock that followed 119 minutes afterward. In this table, released seismic energy, *E*, is calculated as: $\log E = 11.8 + 1.5M$ (Gutenberg & Richter 1956; Kanamori 1983). Notably, the seismic energy released by the aftershocks is large compared to the mainshock for this sequence, which is likely due to the fact that the magnitude difference between the mainshock and largest aftershock is 0.4. Ordinarily, this difference is on the order of 1.2, which is known as Båth's law (Båth 1965; Shcherbakov & Turcotte 2004). However, Båth's law may not be followed, in this case, because the examined Christchurch sequence is only a subsequence of a larger mainshock-aftershock sequence. Figure 3 shows the acceleration-time series of this mainshock-aftershock sequence. Table 2 provides important earthquake motion intensity measures for the mainshock and aftershocks.

Table 1. Details about the 22 February 2011 Christchurch mainshock and its significant aftershocks. R_{hyp} is hypocentral distance is to the Christchurch city-centre (-43.532, 172.6367). In the released seismic energy column, the percentages are ratios of aftershock energy to mainshock energy.

Event	Date	Time	M	Depth (km)	R_{hyp} (km)	Energy (ergs)
Mainshock	22/02/2011	12:51	6.3	6.0	8.9	1.8 E21
Aftershock 1	22/02/2011	13:04	5.8	5.9	9.3	3.2 E20 (17.8%)
Aftershock 2	22/02/2011	14:50	5.9	6.6	11.0	4.5 E20 (25.1%)

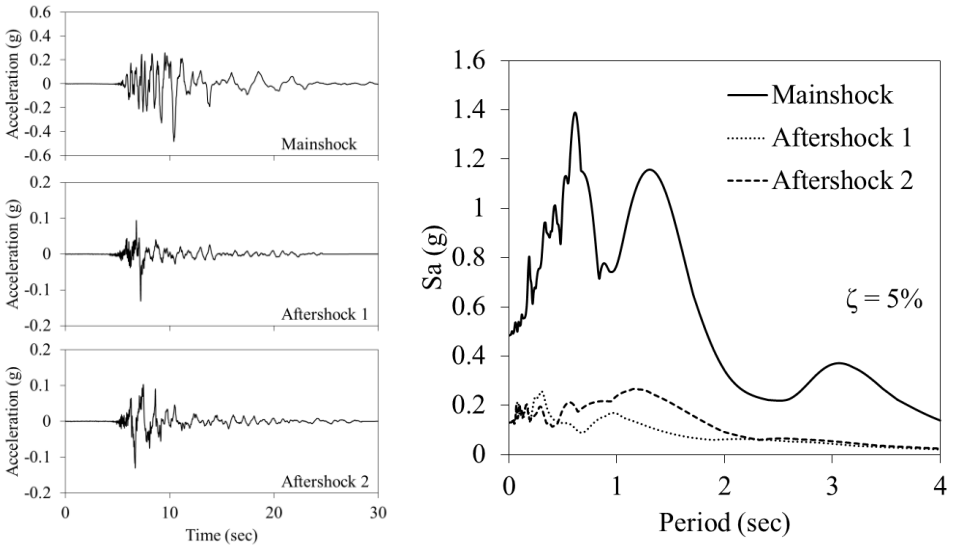

Figure 3. Acceleration-time series and pseudo-spectral acceleration plots for the mainshock and two aftershocks presented in Table 2. The longitudinal (N64E) component from the CCCC seismic station is plotted. The motions have been baseline corrected and bandpass filtered from 0.1 to 25 Hz. Note the difference in vertical scales between the mainshock and two aftershocks.

2.2 **Soil-foundation-structure systems**

Many mid-rise to high-rise buildings in the Christchurch city-centre are reinforced concrete or masonry structures (EERI 2011). Notably, severe seismic damage of these structures – from partial to full collapse – occurred during the 22 February 2011 Christchurch Earthquake sequence (Ingham & Griffith 2011; Kam & Pampanin 2011). In addition to structural damage from strong earthquake motion, significant soil liquefaction also occurred, which led to additional structural damage (Cubrinovski et al. 2011).

Table 2. Earthquake motion intensity measures for the Christchurch mainshock and two subsequent aftershocks [PG(A/V/D) = peak ground (acceleration/velocity/displacement)]. Significant duration defined between 5% and 95% Arias intensity.

Intensity Measure	Mainshock	Aftershock 1	Aftershock 2
PGA (g)	0.483	0.131	0.130
PGV (cm/sec)	71.3	13.7	18.6
PGD (cm)	22.0	4.6	4.5
Arias intensity (m/sec)	2.7	0.06	0.12
Mean period (sec)	1.17	0.916	1.07
Significant duration (sec)	11.32	8.16	8.18

There are some steel structures in the Christchurch city-centre, and most of these steel structures have been constructed in recent years using the latest design codes. In addition, the seismic resisting systems of the steel structures are primarily eccentric bracing frames (EBF). For these reasons, observations of seismic damage to steel structures following the recent New Zealand Earthquakes were rare. A notable exception is a car park, in which a few EBF links were fractured during strong shaking (Bruneau et al. 2011).

In this study, we examine the effects of a mainshock and two aftershocks on a mid-rise EBF building. This examination is completed numerically using the finite-element program OpenSees (McKenna et al. 2010). Due to the difficulty in acquiring structural details of local buildings in the Christchurch city-centre, we chose a generic mid-rise EBF building from the work of Ganuza (2006). The chosen building is a 9-story EBF building designed using the 2003 NEHRP Recommended Provision (BSSC 2003), which was designed considering an active seismic site in Los Angles with a NEHRP site class D (typical of coastal California). With a fixed-base assumption, the design spectral demands of the EBF building presented by Ganuza (2006) are 2.11 g at the short period (0.2 sec) considering a 2% probability of exceedance in 50 years, and 1.08 g at the long period (1 sec) considering a 10% probability of exceedance in 50 years. To compare with the NZS1170 design demands with a similar risk target (e.g., 2500-year earthquake motion return period for a typical site in Christchurch), the short-period demand is about 1.2 g and the long-period demand 0.7 g. Accordingly, the EBF building considered in this study was designed considering higher seismic demands.

In Figure 4a, the schematic plan of the perimeter frame of the 9-story EBF building is provided. Structural design of the superstructure, including the select sections for both moment and gravity frames, are the same as used in the *lam19* model in Ganuza (2006). The design base-shear force is 5.9 MN, or about 0.067 of the weight of the superstructure. To consider soil-foundation-structure interaction, a shallow mat foundation is designed in this study, which is fully embedded with an embedment depth of 1.524 m. Soil parameters are given in Table 3. For this initial modeling effort, the soil is considered to be dry.

Table 3. Soil parameters used for numerical modelling

Parameter	Value	Unit
Dry unit density	1,600	kg/m^3
Small-strain shear modulus	16	MPa
Friction angle	38	degrees
Poisson's ratio	0.3	-

Normal-weight concrete (27.6 MPa) is used to model the basement walls and the mat foundation. The mat foundation is designed with an embedment depth of 1.524 m. The parameters used herein are an oversimplification of the soil-foundation configuration. The described configuration represents a typical rigid mat foundation sitting atop soft soil with a very large vertical factor of safety.

We consider flexibility of the soil-foundation interface (i.e., soil-foundation-structure interaction) during the modelling process. This is accomplished by employing a design-oriented approach using a beam-on-nonlinear-Winkler-foundation (BNWF) model. A BNWF model is constructed of distributed spring elements, which represent a combination of nonlinear springs, gap elements, and dashpots (Boulanger et al. 1999; Raychowdhury & Hutchinson 2008). For the model described within this paper, individual, nonlinear, mechanistic springs – *PySimple2*, *TzSimple2*, and *QzSimple2* – are used to model the lateral foundation sliding, lateral foundation-soil interface friction, and the foundation's vertical uplifting response. The aforementioned springs are characterized using elastic foundation impedance functions (Gazetas 1991). The plastic constitutive relations of the foundation springs are characterized by *back-bone* curves with parameters validated using geotechnical centrifuge-based experiments (Raychowdhury & Hutchinson 2009).

Elastic beam-column elements are used to model all of the superstructure beams, columns, and braces. P-delta effects are considered in the columns. The beam-to-column and the brace-to-frame connections are modelled as pin-connections. Inelastic deformation is assumed to only occur at connections. Plastic hinges are added at the two ends of each connection, wherein uncoupled bilinear shear, elastic bending, and axial tension sections are aggregated. The base nodes of the columns are pin-connected to the nonlinear Winkler foundation beam.

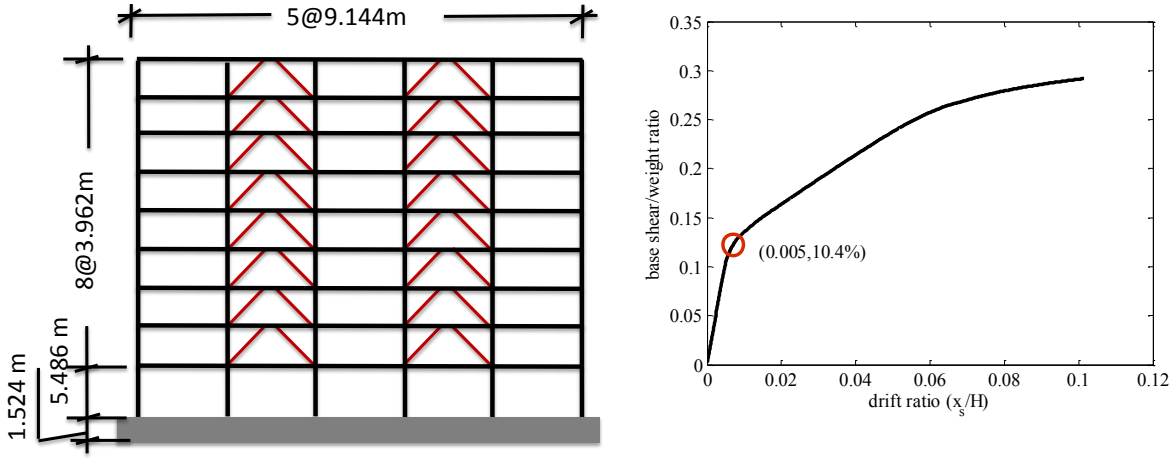

Figure 4. (a) 2D schematic of the perimeter frame of a 9-story EBF building; (b) pushover response of the frame-foundation model.

Nonlinear pushover is obtained to study the lateral global response of the building. As shown in Figure 4b, the drift ratio at the roof of the building plotted against the base shear ratio. A system yield point is extracted at 0.5% drift ratio corresponding to a 10.4% base shear-to-weight ratio.

Eigenvalue analysis is conducted for the fixed-base superstructure and the foundation-structure systems. The fixed-base period, T_1^{fixed}, is 1.76 sec, and the flexible-base period, T_1^{SFSI}, is 1.86 sec. Accordingly, the period lengthening ratio, T_1^{fixed}/T_1^{SFSI}, which correlates well to inertial soil-foundation-structure interaction (Stewart et al. 1999), is approximately 1.06. A period lengthening ratio of 1.06 indicates that at the linear elastic range, the potential soil-foundation-structure interaction is moderate. However, as noted later in this paper, inertial SFSI could be more significant if the soil-foundation interface responds nonlinearly.

Considering T_1^{SFSI}, the obtained spectral demands are shown Table 4. These spectral demands are consistent with the trends of the intensity measures shown in Table 2, reflecting that the mainshock has a much higher demand than the two aftershocks on the structure.

3 PROGRESSIVE DAMAGE SIMULATION

To study the progressive seismic response of the nonlinear foundation-building model, we first use the

non-scaled mainshock and aftershocks records. Due to the underlying significant nonlinearity in the system (foundation springs and plastic EBF link hinges), we use the Hilbert-Hughes-Taylor integration (α = 0.5) method. In addition, a variable transient time step is adopted. To assure that the free vibration is finished prior applying to the aftershocks, an extra 10 sec duration is added to the original records.

Table 4. Spectra demands considering the system period T_1^{SFSI} = 1.86 sec.

	Mainshock	Aftershock 1	Aftershock 2
Sa(T_1) (g)	0.50	0.06	0.13
Sd(T_1) (cm)	41.5	5.2	10.7

In Figure 5, we provide time-series of response demands in terms of the structural-deformation induced ductility demand at the roof and the rigid-body induced 'ductility' demand at the roof due to foundation sliding and rocking. From Figure 5, it is obvious that inelastic structural deformation is produced during the mainshock, because the peak ductility demand is 1.5. Although this relatively low ductility demand implies that no serious structural damage would occur to the building, a residual structural deformation is obtained after the mainshock. Figure 5a shows that the plastic residual is about 0.5 in terms of ductility demand, which translates to approximately 7.4 cm of residual deformation. This residual deformation is carried during the two aftershocks (i.e. the superstructure as a subsystem is dynamically vibrating about a new position), but no further plastic structural deformation is attained during the two aftershocks.

The rigid-body motion due to the inertial SFSI is shown in Figure 5b, which combines both foundation sliding and foundation rocking (i.e., $x_f = x_{sliding} + \theta\, h$; where θ is the foundation rocking and h is height at the roof level). The overall magnitudes of the rigid-body motion are relatively small (i.e., on the order of less than 10% of the ductility demand). However, small foundation plastic deformation – which is primarily induced by foundation sliding – can be observed. The aftershock excitation to the foundation primarily induces linear elastic vibration with a small self-centring after the first aftershock.

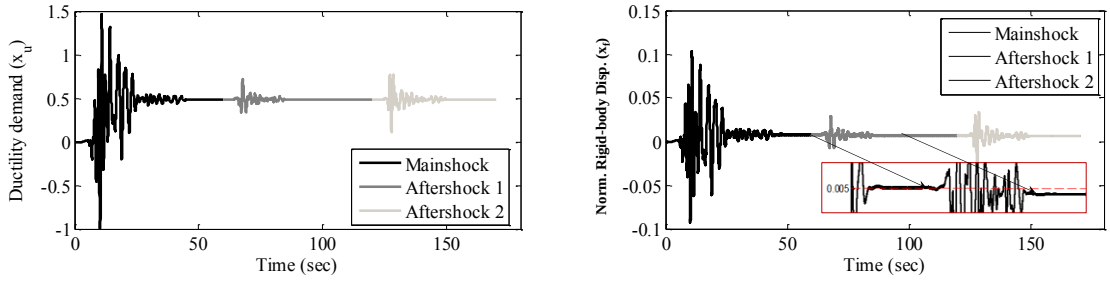

(a) (b)

Figure 5. (a) Ductility demand at the roof due to the lateral structural drift (x_u); (b) Normalized displacement demand of the foundation motion (x_f) including both foundation sliding and rocking. In both figures, the displacement demands are normalized to the yielding drift ratio of the structure (δ_y =5%).

We also examine the force demands at the base of the foundation-structure model. Figure 6a and 6b illustrates the base shear ratio (normalized by the weight of the structure), and the base moment ratio (normalized to the weight of the structure multiplied by the building height), respectively. Figure 6a clearly indicates that the inelastic base shear demands are much higher after the mainshock when compared to the aftershocks. Residual base shear forces – which are on the order of 2% of the weight of the building – are also observed after the mainshock. Considering the foundation force and displacement demands, we further provide the force-displacement relations in Figure 7. From this figure, it can be seen that strong nonlinearity occurs during the mainshock for the sliding model. Correspondingly, approximately linear sliding is observed during the following two aftershocks. For the rocking model, weaker inelasticity is observed during the mainshock followed by elastic rocking during the aftershocks. The hysteresis in the foundation motion during the mainshock, given the

foundation deformation is small, should be considered as a significant energy dissipation mechanism that reduces the overall demands to the system.

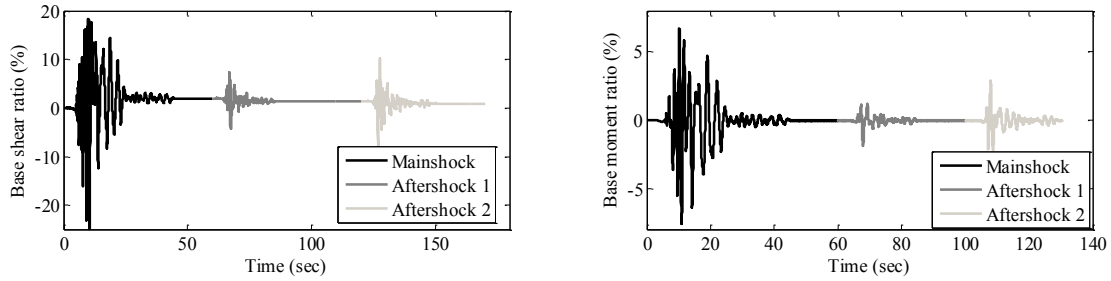

Figure 6. (a) Base shear ratio demands normalized by the total weight; (b) base moment demands.

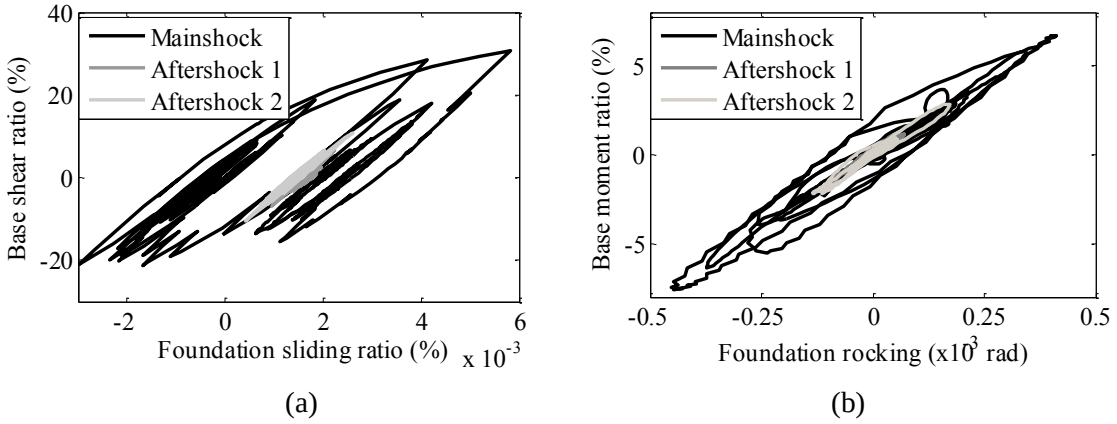

Figure 7. Foundation force-displacement relations: (a) base shear vs. foundation sliding; and (b) basement vs. foundation rocking.

4 CONCLUSIONS

The mainshock-aftershock sequence resulting from the 4 September 2010 Darfield earthquake is examined in this paper. Of primary interest is the subsequence that occurred after the 22 February 2011 Christchurch Earthquake. The close succession of very close and shallow earthquakes caused significant damage to the Christchurch city-centre. This is a progressive damage scenario, and it is currently not accounted for in seismic design.

An eccentrically-braced frame structural model was developed in this paper within the finite-element program OpenSees. Soil-foundation-structure interaction effects were explicitly modelled using nonlinear Winkler springs. The structural model was 9-stories tall and founded on a shallow mat foundation. This type of structure exists in Christchurch as well as other seismically active areas worldwide. The structural model was subjected to the M6.3 22 February 2011 Christchurch mainshock and two closely following aftershocks with magnitudes of 5.8 and 5.9. Results show that for this type of model, most of the structural demand occurs during the mainshock, and little further damage occurs during the successive aftershocks. The first and second major aftershocks occurred 13 and 119 minutes after the mainshock, respectively; therefore, it was impossible to quantitatively estimate building damage immediately after the mainshock. Accordingly, the results of this paper are important, because they indicate that for this type of structure, most of the damage occurred during the mainshock, so the progressive damage scenario is less important. More modelling is needed to examine more structure types (i.e., reinforced concrete and masonry buildings), more soil types, and importantly, to develop important understandings of the sensitivity of important parameters. The authors are currently undertaking this modelling effort.

REFERENCES:

Bannister, S., Fry, B., Reyners, M. Ristau, J. & Zhang, H. 2011. Fine-scale relocation of aftershocks of the 22 February M_w 6.2 Christchurch Earthquake using double-difference tomography, *Seismological Research Letters*. 82 (6). 839-845.

Båth, M. 1965. Lateral inhomogeneities in the upper mantle, *Tectonophysics*. 2. 483-514.

Bhattachatya, P., Phan, M. & Shcherbakov, R. 2011. Statistical analysis of the 2007 M_W 7.9 Denali earthquake aftershock sequence, *Bulletin of the Seismological Society of America*. 101 (6). 2662-2674.

Boulanger, R. W., Curras, C. J., Kutter, B. L., Wilson, D. W. & Abghari, A. 1999. Seismic soil-pile-structure interaction experiments and analyses, Journal of Geotechnical and Geoenvironmental Engineering. 125 (9), 750-759.

Bruneau, M., Clifron, C., MacRae, G., Leon, R. & Fussell, A. 2011. Steel building damage from the Christchurch Earthquake of February 22, 2011, NZST. Multidisciplinary Center for Earthquake Engineering Research (MCEER) Report. University of Buffalo.

BSSC. 2003. NEHRP Recommended Provisions for Seismic Regulations for New Buildings and Other Structures. Building Seismic Safety Council, Washington, DC.

Cubrinovski, M., Bray, J. D., Taylor, M., Giorgini, S., Bradley, B., Wotherspoon, L. & Zupan, J. 2011. Soil liquefaction effects in the central business district during the February 2011 Christchurch Earthquake, Seismological Research Letters. 82 (6). 893-904.

EERI. 2011. The M6.3 Christchurch, New Zealand, Earthquake of February 22, 2011, EERI Special Earthquake Report, Earthquake Engineering Research Institute, Oakland, CA.

Ganuza, E. A. B. 2006. Seismic behavior of hybrid lateral-force-resisting systems, Master of Science thesis, University of Buffalo, Department of Civil, Structural and Environmental Engineering, Buffalo, NY.

Gazetas, G. 1991. Chapter 15: Foundation vibrations, In Foundation Engineering Handbook, Second Edition. H.-Y. Fang, editor. Van Nostrand Reinhold: Norwell, MA.

Gutenberg, B. & Richter, C. F. 1954. *Seismicity of the Earth and Associated Phenomenon*. Princeton, New Jersey: Princeton University Press.

Ingham, J. & Griffith, M. 2011. Performance of unreinforced masonry buildings during the 2010 Darfield (Christchurch, NZ) earthquake, Australian Journal of Structural Engineering. 11 (3). 207-225.

Kagan, Y. Y. 2002. Aftershock zone scaling, *Bulletin of the Seismological Society of America*. 92. 641-655.

Kam, W. Y. & Pampanin, S. 2011. The seismic performance of RC buildings in the 22 February 2011 Christchurch earthquake, Structural Concrete 12 (4). 223-233.

Kanamori, H. 1983. Magnitude scale and quantification of earthquakes, *Tectonophysics*. 93. 185-199.

Lay, T. & Wallace, T. C. 1995. *Modern Global Seismology*. San Diego, California: Academic Press.

McKenna, F., Scott, M. H. & Fenves, G. L. 2010. Nonlinear finite-element analysis software architecture using object composition, *Journal of Computing in Civil Engineering*. 24 (1). 95-108.

Raychowdhury, P. & Hutchinson, T. C. 2008. Nonlinear material models for Winkler-based shallow foundation response evaluation, In Proceedings of the Sessions of GeoCongress 2008. New Orleans, LA.

Raychowdhury, P. & Hutchinson, T. C. 2009. Performance evaluation of a nonlinear Winkler-based shallow foundation model using centrifuge test results, Earthquake Engineering and Structural Dynamics. 38 (5). 679-698.

Shcherbakov, R. & Turcotte, D. L. 2004. A modified form of Båth's law, *Bulletin of the Seismological Society of America*. 94 (5). 1968-1975.

Stewart, J. P., Fenves, G. L. & Seed, R. B. 1999. Seismic soil-structure interaction in buildings. I: Analytical aspects, *Journal of Geotechnical and Geoenvironmental Engineering*. 125 (1). 26-37.